The Southampton Cauchy-characteristic Matching Project

Ray d'Inverno*

Faculty of Mathematical Studies, University of Southampton, Southampton, United Kingdom

Lectures given at the Conference on Gravitational Waves: A Challenge to Theoretical Astrophysics Trieste, 5-9 June 2000

LNS013005

*R.A.d'Inverno@maths.soton.ac.uk

Abstract

The Southampton Numerical Relativity Group have set up a long term project concerned with investigating Cauchy-characteristic matching (CCM) codes in numerical relativity. The CCM approach has two distinct features. Firstly, it dispenses with an outer boundary condition and replaces this with matching conditions at an interface residing in the vacuum between the Cauchy and characteristic regions. A successful CCM code leads to a transparent interface and so avoids the spurious reflections which plague most codes employing outer boundary conditions. Secondly, by employing a compactified coordinate, it proves possible to generate global solutions. This means that gravitational waves can be identified unambiguously at future null infinity. To date, cylindrical codes have been developed which have been checked against the exact solutions of Weber-Wheeler, Safier-Stark-Piran and Xanthopoulos. In addition, a cylindrical code has been constructed for investigating dynamic cosmic strings. Recently a master vacuum axi-symmetric CCM code has been completed which consists of four independent modules comprising an interior Cauchy code, an exterior characteristic code together with injection and extraction codes. The mail goal of this work is to construct a 3 dimensional code possessing the characteristic, injection and extraction modules which can be attached to an interior code based on a finite grid. Such a code should lead to the construction of more accurate templates which are needed in the search for gravitational waves.

1 Cauchy-characteristic matching

One of the major problems in Numerical Relativity is that there is no known exact local expression for gravitational waves - they can only be exactly identified asymptotically (that is out at future null infinity). In most work to date, numerical simulations are carried out on a central finite grid extending into the vacuum region surrounding isolated sources and ad-hoc conditions are imposed at the edge of the grid to prevent incoming waves (which would be unphysical). These ad-hoc conditions are drawn from linearised theory and are not exact and, as a consequence, they generate spurious reflected numerical waves. The basic formalism that these numerical codes employ is the ADM 3+1 formalism in which 4-dimensional space-time is decomposed into a family of constant time 3-dimensional spatial slices threaded by timelike curves. Although this formalism is well adapted to central regions it does not work if the foliation goes null. Yet null foliations are important in the study of gravitational waves since the signals propagate along the null generators of null hypersurfaces.

In contradistinction, the DSS 2+2 formalism [1], [2] is specifically designed to deal with null foliations of space-time. The 2+2 formalism decomposes space-time into two families of spacelike 2-surfaces. We can view this as a constructive procedure in which an initial 2-dimensional submanifold S_0 is chosen in a bare manifold, together with two vector fields v_1 and v_2 which transvect the submanifold everywhere (Fig. 1). The two vector fields can then be used to drag the initial 2-surface

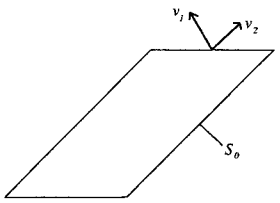

Figure 1: 2-dimensional submanifold and two transvecting vector fields

out into two foliations of 3-surfaces. The character of these 3-surfaces will depend in turn on the character of the two vector fields. Since the two vector fields may each separately be null, timelike or spacelike this gives rise to six different types of decomposition. The most important case for CCM is the null-timelike foliation (Fig. 2).

Cauchy-characteristic matching, or CCM for short, makes use of the null-timelike decomposition in the vacuum region exterior to the sources and in this region the technique of Penrose conformal compactification is used to bring in the points at infinity to a finite position. This, in turn, gives rise to the possibility of generating global numerical codes. In short, CCM consists of combining a central 3+1 nu-

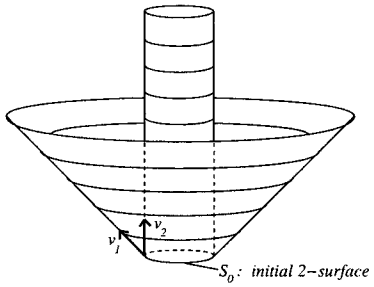

Figure 2: Null-timelike foliation

merical code with an exterior null-timelike 2+2 code connected across a timelike interface residing in the vacuum. In addition, the exterior region is compactified so as to incorporate null infinity where gravitational radiation can be unambiguously defined. The compactified picture is shown schematically in Fig. 3.

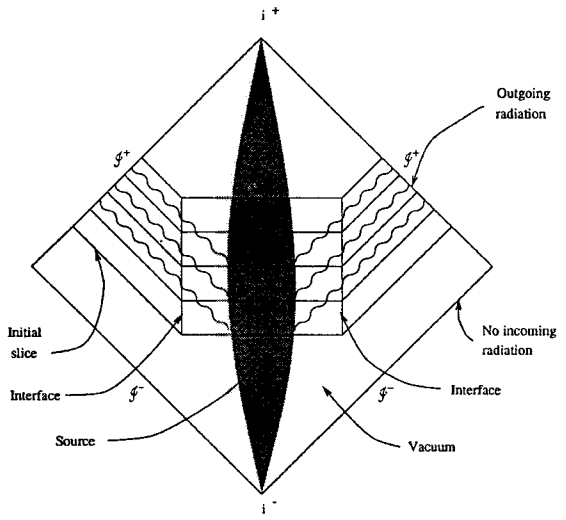

Figure 3: Conformal picture of Cauchy-characteristic matching

In the exterior characteristic region the Einstein field equations reduce to a hierarchical system of ordinary differential equations, which are easier and less expensive to solve than corresponding partial differential equations. Moreover, Bishop et al. [3] have shown that CCM is a preferred method if one is interested in constructing increasingly accurate solutions. When CCM works it essentially overcomes the outer boundary problem of finite codes by replacing the outer boundary with a *transparent* interface which allows gravitational waves to pass through without modification. However, there is a considerable price to pay for this improvement. First of all the mathematics of the asymptotic region is quite complicated in the

general case and the interface equations for matching the metric and its derivatives are both complicated and computationally expensive. CCM codes have been reviewed in [4]. In the longer term, it might prove most effective to base codes on hyperboloidal surfaces [5], that is spacelike surfaces which are asymptotically null. This one family of hypersurfaces would not then involve any interface and yet would still generate the exact asymptotic forms for the gravitational waves.

2 The Southampton CCM Project

There are two main groups which have investigated CCM. One is centred at Pittsburgh under the leadership of Jeff Winicour and has included coworkers Roberto Gomez, Nigel Bishop and Philippos Papadopoulos, among others. The other is at Southampton under the leadership of Ray d'Inverno and has included coworkers James Vickers, Mark Dubal, Chris Clarke, Elizabeth Sarkies, Denis Pollney, Uli Sperhake and Robert Sjödin. The Southampton Project is a longterm project directed at applying the CCM approach to scenarios of astrophysical interest. It started by demonstrating the viability of the approach in the case of the wave equation in flat space, that is in the absence of gravitation [6]. One of the weaknesses of Numerical Relativity is that there are very few exact solutions which can be used to check the accuracy of a numerical code. In the next stage we looked at vacuum cylindrical symmetry as a prototype system with one spatial degree of freedom [7]. This has resulted in a considerable body of work and we have been able to check our codes out against a number of exact solutions. The main theoretical tool employed was that of Geroch decomposition, which essentially reduces the dimensionality of the problem by factoring out the z-direction. The vacuum cylindrical code was first compared with a non-rotating exact solution due to Weber and Wheeler and agreement was found to be better than 0.1% [8]. The significance of this work can best be appreciated when it is compared to using a standard outgoing wave condition at various distances from the axis of symmetry. Of course, the further out this condition is imposed then the greater the accuracy of the resulting evolution. Fig. 4 shows how well CCM compares with outgoing radiation conditions imposed at a number of different radii.

The agreement with the exact Weber-Wheeler solution has been improved by two orders of magnitude in some recent work [9], [10] (see section 3). Asymptotically, a gravitational wave is purely transverse in character and has two polarisation states which are known as "+" and "x". The code was used to investigate "colliding" cylindrical gravitational waves which have different mixtures of ingoing and outgoing modes. The code was then modified and used to check a much more complicated exact rotating solution due to Piran, Safier and Katz [11]. This is a more exacting test of the CCM method since it involves passing derivative information across the interface, but again the approach appears to be viable. It proved necessary

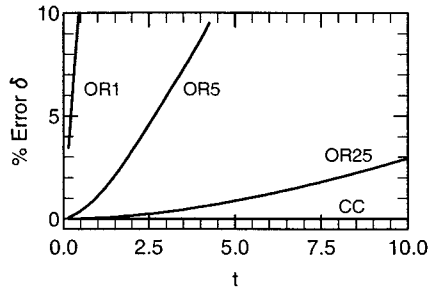

Figure 4: The % error for Weber-Wheeler of CCM (CC) compared with the a code employing the outgoing radiation condition applied at r=1 (OR1), r=5 (OR5) and r=25 (OR25)

to modify the code in order to cope with the asymptotic singular nature of the rotational degree of freedom. Again the results have been improved by two orders of magnitude [9], [10] and extended to another exact solution due to Xanthopoulos [12] which also has both gravitational degrees of freedom present.

Attention then turned to investigating axially symmetric systems, that is systems possessing two spatial degrees of freedom. It was hoped that in doing this we would be able to confirm and improve upon the classic results of Stark and Piran [13]. They combine a radial gauge with polar slicing and this approach has been hard-wired into our vacuum axisymmetric CCM code. It was necessary first to match the metric and its first derivatives across the interface [14]. It is not clear a priori that this is even possible, because the geometries are so profoundly different in each region. It turned out that it was possible once we had understood better the nature of polar slicing [15]. The second requirement is to show that it is possible to compactify the exterior region in such a way that the field equations remain regular and that logarithmic singularities do not occur [16]. The analysis involved is quite delicate and the resulting equations are particularly complicated. For example, the one governing the mass loss of the system asymptotically involves over 1,000 terms. In order to carry out these calculations use was made of the computer algebra system SHEEP [17].

In the final stage of the Southampton Project, attention will be turned to fully 3 dimensional dynamical systems. The belief is that the code will need little alteration in the characteristic region and will merely involve dropping the ϕ-invariance (where ϕ is the usual azimuthal angle of axial symmetry).

3 Cylindrically symmetric exact solutions

For the case of a cylindrically symmetric vacuum spacetime one can write the metric in Jordan, Ehlers, Kundt and Kompaneets (JEKK) form [18] [19]

$$ds^2 = e^{2(\gamma-\psi)}(dt^2 - d\rho^2) - \rho^2 e^{-2\psi} d\phi^2 - e^{2\psi}(\omega d\phi + dz)^2. \tag{1}$$

The metric functions ψ and ω encode the longitudinal and rotational degrees of freedom. The function γ is related to the "energy" of the solution and is determined from ψ and ω by quadrature. The line element is independent of ϕ and z and is invariant under the transformation $(\phi, z) \longmapsto (-\phi, -z)$. In terms of these variables we find the norm of the Killing vector in the z-direction $\xi^\mu = \delta^\mu_3$ to be given by

$$\nu = -\xi^\mu \xi_\mu = e^{2\psi}, \tag{2}$$

and the Geroch twist potential τ is related to the rotational degree of freedom ω by

$$D_a \tau = \rho^{-1} e^{4\psi}(\omega_{,\rho}, \omega_{,t}, 0, 0). \tag{3}$$

The null geodesics for the JEKK line element are given by the simple conditions $u = t - \rho =$ constant and $v = t + \rho =$ constant. In the characteristic region we adopt the coordinates (u, y, ϕ, z) where y is the compactified coordinate

$$y = \frac{1}{\sqrt{\rho}}. \tag{4}$$

The basic technique for regularising the equations is to work in terms of the Geroch potential τ. In the early work, τ was used solely in the characteristic region, but in the more recent work it was used in both regions. We present some results below.

3.1 The Weber-Wheeler solution

The Weber–Wheeler solution [20] consists of a cylindrically symmetric vacuum gravitational wave with one radiational degree of freedom corresponding to the + polarisation mode asymptotically [21]. It describes a gravitational pulse originating from past null infinity and moving toward the z-axis. After imploding on the axis, it emanates to future null infinity. This solution has no rotation so that ω and hence τ vanish and the solution may be described in terms of ψ which satisfies the wave equation. A solution to the wave equation in cylindrical coordinates may be given in terms of Bessel functions and by superposing such solutions we may write

$$\psi(t, \rho) = 2b \int_0^\infty e^{-a\Omega} J_0(\Omega\rho) \cos(\Omega t) d\Omega, \tag{5}$$

where $a > 0$. Following the notation of [9], we let

$$X = a^2 + \rho^2 - t^2, \tag{6}$$

and one may show that (5) may be written in the alternative form

$$\psi(t, \rho) = b\sqrt{\frac{2(X + \sqrt{X^2 + 4a^2t^2})}{X^2 + 4a^2t^2}}. \tag{7}$$

The corresponding value of γ may be found by integrating the field equations and, using $\gamma(t, 0) = 0$, we find

$$\gamma(t, \rho) = \frac{b^2}{2a^2}\left[1 - 2a^2\rho^2\frac{X^2 - 4a^2t^2}{(X^2 + 4a^2t^2)^2} - \frac{a^2 + t^2 - \rho^2}{\sqrt{X^2 + 4a^2t^2}}\right]. \tag{8}$$

To plot the solution for $0 \leq \rho < \infty$ we introduce the radial variable

$$w = \begin{cases} \rho & \text{for } 0 \leq \rho \leq 1, \\ 3 - 2y & \text{for } 0 \leq y \leq 1, \end{cases} \tag{9}$$

and so $0 \leq z \leq 3$. This choice is slightly different from that of Dubal et al. [8] and avoids discontinuities in the radial derivatives at the interface due to the square root in the definition of y. Plots are given in Fig. 5 of ν, the norm of the Killing vector its error scaled up by an appropriate factor. Note how the error virtually disappears once the wave has dissipated.

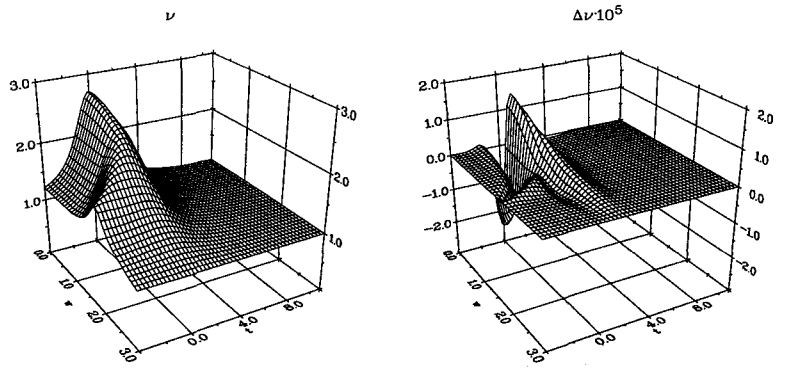

Figure 5: Plots of $\nu(t, w)$ and the error $\Delta\nu(t, w) \cdot 10^5$ for the Weber-Wheeler solution for $-4 \leq t \leq 10$ and $a = 2$, $b = 0.5$.

3.2 The Xanthopoulos solution

The next solution we consider is one due to Xanthopoulos [12] which has both gravitational degrees of freedom present. It fails to be vacuum on the z-axis where

it has a conical singularity and therefore describes a rotating vacuum solution with a cosmic string type singularity. Xanthopoulos derived the spacetime by finding a solution to the Ernst equation in prolate spheroidal coordinates. To make use of the cylindrical code, we must transform to cylindrical coordinates and also find the Geroch potential. It is convenient to first define the following quantities [9]

$$Q = \rho^2 - t^2 + 1, \tag{10}$$

$$X = \sqrt{Q^2 + 4t^2}, \tag{11}$$

where $0 < |a| < \infty$. The norm of the Killing vector in the z-direction is then given by

$$\nu(t,\rho) = \frac{\frac{1}{2}[(2a^2+1)X + Q] - 1}{\frac{1}{2}[(2a^2+1)X + Q] + 1 - a\sqrt{2(X-Q)}}. \tag{12}$$

The Geroch potential τ is easily obtained from the Ernst potential and is found to be

$$\tau(t,\rho) = -\frac{\sqrt{2(a^2+1)}\sqrt{X+Q}}{\frac{1}{2}[(2a^2+1)X + Q] + 1 - a\sqrt{2(X-Q)}}. \tag{13}$$

Expressions for all these quantities may be obtained in the exterior characteristic region by transforming to the (u, y) variables. Although ψ tends to zero as one approaches null infinity, ω diverges so that the 4-dimensional metric is not asymptotically flat even along null geodesics lying in the planes z = constant. However by contrast the Geroch potential τ vanishes as one approaches null infinity in the 3-dimensional spacetime. This is an example of the fact that the Geroch potential can be well behaved even if ω in the JEKK form of the 4-metric diverges as one goes outward in a null direction [9].

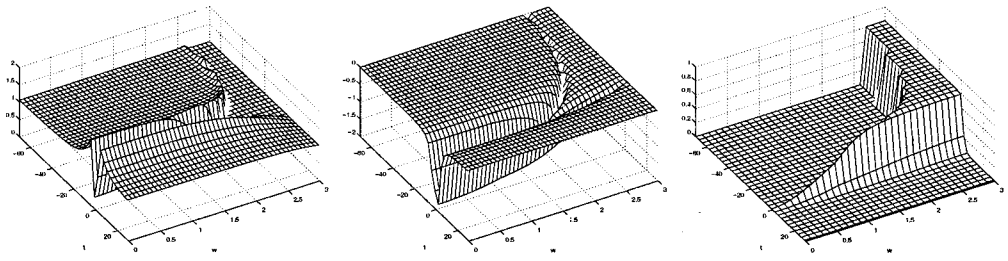

Figure 6: The Xanthopoulos solution for $-70 \leq t \leq 30$, $0 \leq w \leq 3$ and $a = 0.5$. Plots are from left to right: $\nu(t,w)$, $\tau(t,w)$ and $\gamma(t,w)$. One clearly sees the incoming pulses in ν and τ. As the pulse hits the axis is hit the string loses energy through gravitational radiation as seen in γ.

In order to analyse the accuracy of the code, we define the pointwise error at the ith time slice and jth grid point for some function f by [9]

$$\xi_j^i(f) = f(t_i, w_j)_{\text{exact}} - f(t_i, w_j)_{\text{computed}}. \tag{14}$$

The pointwise error for the Xanthopoulos solution is shown in Fig. 7 for 600 grid points and 10,000 time steps corresponding to $0 \leq t \leq 15$. The code is very stable and accurate for at least 20,000 time steps, and beyond this point the metric functions have almost decayed to zero and the dynamics is very slow. The code is second order convergent in both time and space.

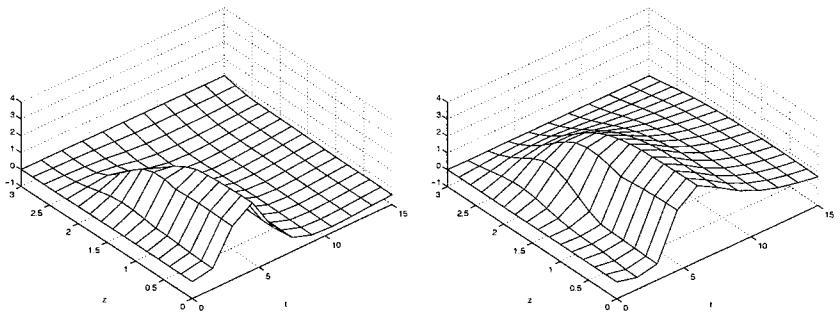

Figure 7: Pointwise error for the Xanthopoulos solution. From left to right: $\nu(t,z) \cdot 10^5$ and $\tau(t,z) \cdot 10^5$.

3.3 The Piran-Safier-Katz solution

The next exact solution is one due to Piran et al. [11] which also has two degrees of freedom representing the two polarisation states. As in the case of Xanthopoulos solution, it represents two incoming pulses that implode on the axis and then move away from it. Piran et al. obtained their solution by starting with the Kerr metric in Boyer-Linquist form, transforming to cylindrical polar coordinates and then swapping the t and z coordinates (and introducing some factors of i to maintain a real Lorentzian metric). The resulting metric may be written in JEKK form. The solution depends on two parameters a and b where $1 \leq a < \infty$ and $0 < b < \infty$. Minkowski space-time is obtained in the limit $a \to 1$, and we can also consider the case $b \to 0$, in which case the rotation vanishes. This was not true for the Xanthopoulos solution which is only real for a sufficiently large rotation. The solution is regular on the axis, but like the Xanthopoulos solution, the metric function ω diverges as one approaches null infinity. Again the answer is to transform to the ν, τ variables which are regular both on the axis and at null infinity. Finding ν is straightforward; however solving the differential equations for the Geroch potential τ for such a complicated metric is extremely difficult, but τ may be found by first finding the Geroch potential for the timelike Killing vector of the Kerr solution and then making the appropriate transformations. Note that the same process

transforms the Killing vector into one along the z-axis. One then finds [9]:

$$\nu(t,\rho) = \frac{a^2(1-RS)^2 + (R+S)^2}{a^2T^2 + (R-S)^2}, \tag{15}$$

$$\tau(t,\rho) = -\frac{4\sqrt{(a^2-1)RS}(R-S)}{[2\sqrt{(a^2-1)RS} + a(1+RS)]^2 + (R-S)^2}. \tag{16}$$

where

$$R = b^{-1}[\sqrt{b^2 + (t-\rho)^2} - t + \rho], \tag{17}$$

$$S = b^{-1}[\sqrt{b^2 + (t+\rho)^2} + t + \rho], \tag{18}$$

$$T = 1 + RS + 2a^{-1}\sqrt{(a^2-1)RS}, \tag{19}$$

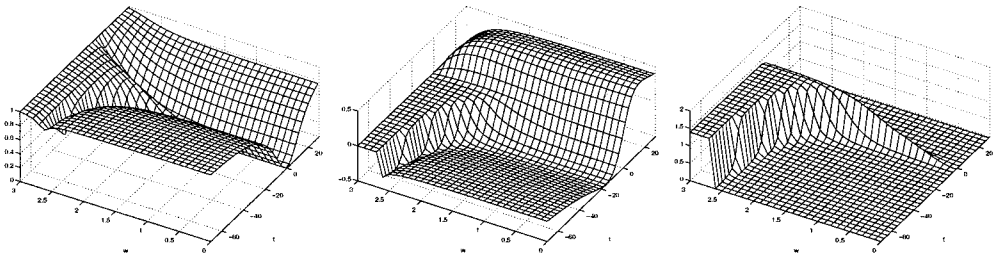

Figure 8: The Piran et al. solution for $-70 \leq t \leq 30$, $0 \leq z \leq 3$, $a = 4$ and $b = 2$. Plots are from left to right: $\nu(t,z)$, $\tau(t,z)$ and $\gamma(t,z)$. Notice that ν does not have a double ridge as found in the Xanthopoulos solution.

The pointwise error for the Piran et al. vacuum solution is shown in Fig. 9 for 600 grid points and 10,000 time steps corresponding to $0 \leq t \leq 15$ [9]. The code is again very stable and accurate for at least 20,000 time steps, and beyond this point the metric functions have almost decayed to zero and the dynamics is very slow. The code is second order convergent in both time and space.

4 Dynamic Cosmic Strings

Cosmic strings are topological defects that formed during phase transitions in the early universe. They are important because they produce a density perturbation in the early universe that can result in the formation of galaxies and other large scale structures [22]. They are also important since they are thought to be sources of gravitational radiation due to rapid oscillatory motion [23]. In the simplest case of a string moving in a fixed background one can take the thin string limit and the dynamics are given by the Nambu–Goto action [24] which is known to admit oscillatory solutions. However in order to fully understand the behaviour of cosmic

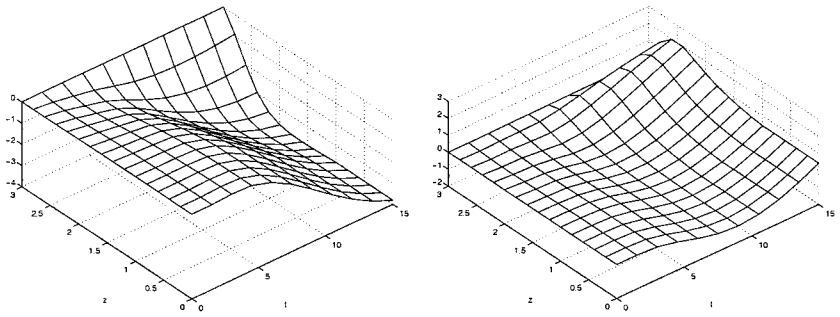

Figure 9: Pointwise error for the Piran et al. solution. From left to right: $\nu(t,z)\cdot 10^5$ and $\tau(t,z)\cdot 10^5$.

strings one should study the field equations for a cosmic string coupled to Einstein's equations. A cosmic string is described by a U(1) gauge vector field A_μ coupled to a complex scalar field $\Phi = 1/\sqrt{2}Se^{i\psi}$. The Lagrangian for these coupled fields is given by

$$L_M = \frac{1}{2}\nabla_\mu S\nabla^\mu S + \frac{1}{2}S^2(\nabla_\mu\psi + eA_\mu)(\nabla^\mu\psi + eA^\mu) - \lambda(S^2-\eta^2)^2 - \frac{1}{4}F_{\mu\nu}F^{\mu\nu}, \quad (20)$$

where $F_{\mu\nu} = \nabla_\mu A_\nu - \nabla_\nu A_\mu$ and e, λ and η are positive coupling constants. In the case of cylindrical symmetry, we need to adopt an ansatz which is an obvious generalisation of the form used by Garfinkle [25], namely

$$\Phi = \frac{1}{\sqrt{2}}S(t,\rho)e^{i\phi}, \quad (21)$$

$$A_\mu = \frac{1}{e}[P(t,\rho)-1]\nabla_\mu\phi. \quad (22)$$

In some recent work from members of the Southampton group, CCM has been used to investigate the effect of a pulse of gravitational radiation on an initially static cosmic string and the corresponding gravitational radiation that is emitted as a result of oscillations in the string [9], [10]. In fact two numerical schemes were employed. The first was an explicit CCM scheme similar to that employed by Dubal et al. [8] and d'Inverno et al. [26]. However, the use of the geometrical variables ν and τ in both the interior Cauchy region and the exterior characteristic region significantly improves the interface and results in a genuinely second order scheme with good accuracy even with both polarisations present. For the vacuum equations the code also exhibits long term stability. However, when the matter variables are included this code performs less satisfactorily. This is because of the existence of exponentially growing non-physical solutions. It is possible to control these diverging solutions by multiplying the u-derivatives of the matter variables

by a smooth 'bump function' which vanishes at $y = 0$ but is equal to 1 for $y > c$ (where c is a parameter). This produces satisfactory results but the bump function introduces some noise into the scheme which eventually gives rise to instabilities. A much better solution is to control the asymptotic behaviour of the numerical solution by using an implicit scheme which solves the main problem with the system of differential equations, namely the irregularity of the equations at both the origin and null infinity.

One case considered is that of a Weber-Wheeler pulse which comes in from past null infinity and interacts with a cosmic string in its static equilibrium configuration. This interaction causes the string to oscillate which, in turn, effects the gravitational field as measured by ν and τ. The oscillations in both S and P decay as one approaches null infinity. After the oscillations have died away the string variables S and P return to their static values. Note that this decay is rather slow and being able to show this effect depends upon the long term stability of the code. The exact strength of the interaction between the string and the gravitational field depends upon the value of η which for typical grand unified theories is about 10^{-3}. For values much lower than this the interaction is so weak that it is hard to observe the effect on the metric variables, but for values of η up to $\eta = 0.1$ the qualitative behaviour remains the same. The amplitude of the oscillations in the string also depends upon the strength of the pulse of gravitational radiation as measured by the width and amplitude of the Weber-Wheeler wave, but again the qualitative features remain similar for a wide parameter range. The string develops a ringing behaviour which, for typical values of the parameters $\alpha = e^2/\lambda = 1$ and $\eta = 10^{-3}$, may be clearly seen in the following plots.

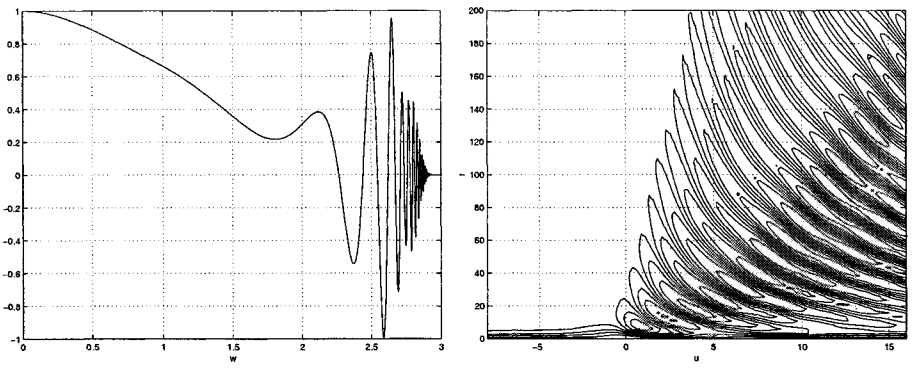

Figure 10: On the left: $P(u, w)$ for $\alpha = 1$, $\eta = 10^{-3}$ and $u = 8.56$. On the right: the corresponding contour plot of $P(u, w)$.

An investigation of the frequencies f_X and f_P of the oscillations of the scalar field S and the vector field P indicate that they are relatively insensitive to the value

of η and the Weber-Wheeler pulse which excites the string. Indeed, it is found that

$$\begin{aligned} f_S &\sim \eta\sqrt{\lambda}, \\ f_P &\sim \eta e. \end{aligned} \tag{23}$$

If we now use the fact that the masses of the scalar and vector fields are given by $m_S^2 \sim \lambda\eta^2$ and $m_P^2 \sim e^2\eta^2$ then this gives

$$\begin{aligned} f_S &\sim m_S, \\ f_P &\sim m_P. \end{aligned} \tag{24}$$

These results were first obtained from numerical investigations but, in fact, it has proved possible subsequently to largely establish these results analytically. Further details may be found in [9] and [10].

5 Waves in a spherical perfect fluid

This work looks at a perfect fluid with stress-energy tensor

$$T_{\mu\nu} = \rho_* w v_\mu v_\nu + p g_{\mu\nu}, \tag{25}$$

where ρ_*, $w = 1 + e + p/\rho_*$ and p are, respectively, the rest mass density, the relativistic enthalpy and the thermal pressure (all measured in the fluid co-moving frame), e is the specific internal energy and v^μ is the fluid 4-velocity, supplemented by the equation of state

$$p = (\Gamma - 1)\rho_* e. \tag{26}$$

The assumption of spherical symmetry leads to the interior form for the line element in Cauchy coordinates (t, r, θ, ϕ),

$$ds^2 = -\alpha^2(r,t)dt^2 + a^2(r,t)dr^2 + r^2 d\Omega^2, \tag{27}$$

and, on the characteristic side, the line element in Bondi coordinates $(u, \tilde{r}, \theta, \phi)$,

$$ds^2 = -\frac{Ve^{2\beta}}{\tilde{r}}du^2 - 2e^{2\beta}du d\tilde{r} + \tilde{r}^2 d\Omega^2, \tag{28}$$

where $V = V(u, \tilde{r})$ and $\beta = \beta(u, \tilde{r})$ only. The spherical symmetry means that one can write down explicit formulae connecting first and second derivatives of the metric variables at the interface [27].

The Einstein field equations are discretized using finite-difference methods which are accurate to second-order in the grid space and time intervals. The evolution equations in the Cauchy region can be written in the form

$$\frac{\partial \mathcal{U}}{\partial t} + 3\frac{\partial}{\partial r^3}(r^2\mathcal{F}) + \mathcal{S} = 0. \tag{29}$$

The equation is differenced using a two-step, predictor-corrector MacCormack scheme [29]. In the characteristic region the evolution equations can be written in the non-conservative form,

$$\frac{\partial \mathcal{U}}{\partial u} + \mathcal{A}\frac{\partial \mathcal{U}}{\partial y} + \mathcal{S} = 0, \tag{30}$$

where $\mathcal{S}$ may contain spatial derivatives of the other variables, and it is simple to modify the MacCormack difference scheme for this type of equation.

In Newtonian theory stars are often described as static polytropic gas spheres with equation of state $p = K\rho^{\Gamma}$. A solution of considerable interest is the case $\Gamma = 6/5$ for which the matter extends to infinity, but the total mass is finite. A relativistic analogue of this solution was obtained by Buchdahl [28]. The initial data which is evolved numerically in this work consists of the Buchdahl solution perturbed by a Gaussian pulse. Moreover, it turns out that in non-symmetrical situations it is very difficult to follow the fluid-vacuum interface and so the approach adopted is to replace the vacuum region by one of very low density material [13], [30], [31]. Typically, the "vacuum" level is around 10^{-10} times that of the peak value of the variable in the initial data set. The initial fluid distribution is then described by a Gaussian pulse, while the low density exterior region is initially taken to be asymptotic to the finite mass static solution of Buchdahl.

We have constructed a CCM code to investigate two general scenarios. The first describes configurations where the fluid flow is predominately outwards, crossing the interface from the Cauchy region into the characteristic region. In the second case the initial conditions are arranged so that the fluid collapses inwards, leading to black hole formation. Examples of the results for a black hole run are shown in Fig. 11. In the radial-polar gauge the formation of a black hole is indicated by a rapid increase of the metric function a, and a corresponding rapid decrease of the lapse α. In spherical symmetry the peak of a asymptotically approaches the horizon and therefore the radius of the black hole can be approximated. Here the black hole radius is $r_{BH} = 0.87$ which is not far from the interface at $r_0 = 1$. In the asymptotic region the solution is once again an outflow as can be seen in Fig. 11(b). Note that the time-step is reduced as the black hole forms to maintain accuracy. This can be seen in the surface plots as the lines become closer in the time direction. The configuration evolves to about $13M$ after which the rapid increase in a halts the code.

The resulting CCM code is second order convergent and stable over long periods. There is no problem evolving the motion of the fluid until either it has moved off the Cauchy portion of the grid (and the code is then evolving the residual low density fluid) or until a black hole has formed. Furthermore there appear to be no significant discontinuities of the variables or their derivatives either at the interface or the junction between the fluid and the background.

One of the problems of dealing with the fluid-vacuum interface by replacing it

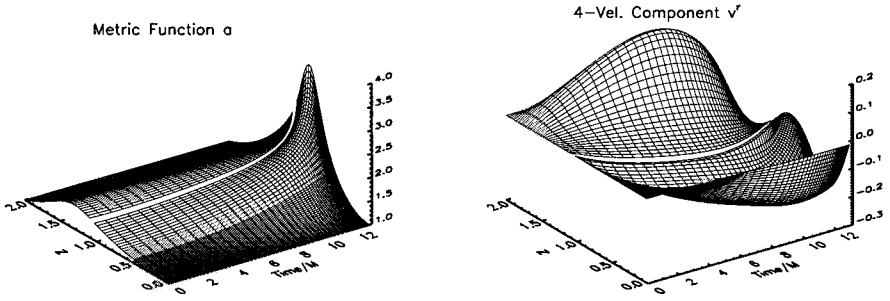

Figure 11: Time evolution of initial data forming a black hole showing (a) the metric function a, and (b) the v^r component of the fluid 4-velocity. Black hole hole formation is indicated by a steep increase in a.

with a low density background when using a traditional 3+1 code is that it involves the use of outer boundary conditions at the edge of the grid. These must deal with the inflow and outflow of matter as well as ensuring outgoing gravitational radiation. Such a procedure can be very problematic, especially in the case of significant inflow. To minimise these problems the Cauchy grid has to be taken to be very large, extending well beyond the boundary of the star, so that the boundary conditions can be applied in a region of very low density. A significant advantage in using CCM is the avoidance of having to apply such a boundary condition. This allows the Cauchy region to be quite small and it is shown in this work that there is no problem locating the interface in a region where there is a significant fluid density. This shows the viability of using CCM to extract gravitational wave information from a small Cauchy region.

6 Principle null directions

Visualisation is of central importance in Numerical Relativity. A constant complaint made by relativists who do not work directly in the field of Numerical Relativity is that visualisation often involves displaying coordinate-dependent information such as metric components. It is not the metric tensor which directly tracks the gravitational field, but rather the Riemann tensor. In vacuum the Riemann tensor reduces to the Weyl tensor and in matter regions it encodes the Ricci tensor, which directly relates to the energy-momentum of the sources present. Again, the components of the Riemann tensor are coordinate-dependent, but the physical information may be extracted from it by constructing the frame components in some canonically defined frame. In some pioneering work [32], Gunnarsen et al. propose using the principal null directions (PNDs) as an interpretive tool in Numerical Relativity. In

vacuum, these provide nearly as much information as the entire Riemann tensor and, moreover, this information is gauge-invariant. Moreover, the peeling theorem of Sachs means that PNDs are natural constructs to investigate asymptotically flat radiative spacetimes [37]. Gunnarsen et al. present a method which assumes as input the intrinsic metric and extrinsic curvature of a spacelike hypersurface and use the d'Inverno–Russell-Clark algorithm [33] to compute the PNDs. The method is therefore clearly adapted to standard 3+1 Numerical Relativity. We outline the algorithm below.

We decompose the Weyl tensor into its electric part $E_{\alpha\beta}$ and magnetic part $B_{\alpha\beta}$. which can be shown to be given in standard 3+1 notation by

$$E_{\alpha\beta} = N^{-1}\mathcal{L}_n K_{\alpha\beta} + K_{\alpha\beta}K^{\gamma}{}_{\beta} + N^{-1}D_\alpha D_\beta N, \tag{31}$$

$$B_{\alpha\beta} = \epsilon_{\alpha}{}^{\lambda\mu} D_\lambda K_{\mu\beta}, \tag{32}$$

where N is the lapse, $K_{\alpha\beta}$ is the extrinsic curvature, $\mathcal{L}_n$ is the Lie derivative in the direction normal to the constant time slice Σ, D_α is the intrinsic covariant derivative in Σ and the tensor $\epsilon_{\alpha\beta\gamma} = \epsilon_{[\alpha\beta\gamma]}$ satisfies $\epsilon_{\alpha\beta\gamma}\epsilon^{\alpha\beta\gamma} = 3!$. The next step is to choose a unit vector $\hat{z}^\alpha$ in Σ and to decompose $E_{\alpha\beta}$ and $B_{\alpha\beta}$ into components along and perpendicular to $\hat{z}^\alpha$. We set

$$\begin{aligned}
e &= E_{\alpha\beta}\hat{z}^\alpha\hat{z}^\beta, && (33)\\
e_\alpha &= E_{\beta\gamma}\hat{z}^\beta\big(\delta_\alpha{}^\gamma - \hat{z}_\alpha\hat{z}^\gamma\big), && (34)\\
e_{\alpha\beta} &= E_{\gamma\delta}\big(\delta_\alpha{}^\gamma - \hat{z}_\alpha\hat{z}^\gamma\big)\big(\delta_\beta{}^\delta - \hat{z}_\beta\hat{z}^\delta\big) + \tfrac{1}{2}e s_{\alpha\beta}, && (35)\\
b &= B_{\alpha\beta}\hat{z}^\alpha\hat{z}^\beta, && (36)\\
b_\alpha &= B_{\beta\gamma}\hat{z}^\beta\big(\delta_\alpha{}^\gamma - \hat{z}_\alpha\hat{z}^\gamma\big), && (37)\\
b_{\alpha\beta} &= B_{\gamma\delta}\big(\delta_\alpha{}^\gamma - \hat{z}_\alpha\hat{z}^\gamma\big)\big(\delta_\beta{}^\delta - \hat{z}_\beta\hat{z}^\delta\big) + \tfrac{1}{2}b s_{\alpha\beta}, && (38)
\end{aligned}$$

where

$$s_{\alpha\beta} = {}^3g_{\alpha\beta} - \hat{z}_\alpha\hat{z}_\beta. \tag{39}$$

The Newman-Penrose Ψs are then given by

$$\begin{aligned}
\Psi_0 &= \big(-e_{\alpha\beta} + J_\alpha{}^\gamma b_{\beta\gamma}\big)m^\alpha m^\beta, && (40)\\
\Psi_1 &= \frac{1}{\sqrt{2}}\big(e_\alpha - J_\alpha{}^\gamma b_\gamma\big)m^\alpha, && (41)\\
\Psi_2 &= \tfrac{1}{2}(-e + ib), && (42)\\
\Psi_3 &= -\frac{1}{\sqrt{2}}\big(e_\alpha + J_\alpha{}^\gamma b_\gamma\big)\bar{m}^\alpha, && (43)\\
\Psi_4 &= \big(-e_{\alpha\beta} + J_\alpha{}^\gamma b_{\beta\gamma}\big)\bar{m}^\alpha\bar{m}^\beta, && (44)
\end{aligned}$$

where $J_\alpha{}^\beta = \epsilon_\alpha{}^{\beta\gamma}\hat{z}_\gamma$ is a rotation by 90 degrees in the plane orthogonal to $\hat{z}^\alpha$, and $m^\alpha = 1/\sqrt{2}(\hat{x}^\alpha - i\hat{y}^\alpha)$ for some pair of orthogonal unit vectors which span that

plane. PNDs are then complex solutions of the quartic

$$\Psi_4 z^4 + 4\Psi_3 z^3 + 6\Psi_2 z^2 + 4\Psi_1 z + \Psi_0 = 0. \tag{45}$$

Since everything is defined in terms of the induced metric on Σ and the extrinsic curvature of Σ (which are known at each stage of a 3+1 numerical evolution), we have presented an algorithm for computing the projections of PNDs within Σ.

In some recent work [34], we have extended this method to both a null 3+1 and a 2+2 formulation. We will not discuss the details here since they are rather extensive. This work has involved some quite deep theoretical investigation of canonical forms for Riemann tensors. As an example of its application, we have utilized this extended method to first investigate the exact cylindrically symmetric solutions of Section III. Here the computed PNDs are stable and can be used to track the ingoing and outgoing cylindrical gravitational waves. We believe that this method may well prove to play an important role in the future for visualisation in Numerical Relativity quite generally.

7 The master axially symmetric vacuum CCM code

In the mid-1980s, the numerical evolution of matter fields in axisymmetry was visited by Stark and Piran [13]. Their code was tested in both vacuum and matter configurations, and was used to compute the gravitational radiation emitted from a collapsing black hole based on a formalism developed in [35] which took special care to construct ADM-type equations which could be reliably implemented in a stable manner. Further, their evolution variables were chosen for their well-defined behaviour at both the inner (r=0) and outer boundaries, and at the poles where axisymmetric codes have traditionally encountered difficulties. At the outer boundary, the choice of variables allowed the two independent polarisation amplitudes of emitted radiation to be easily extracted to good approximation. These strengths suggested that a code based on the methods of Stark and Piran would form a good basis for the Cauchy evolution module of an axisymmetric CCM code.

The line element in the Cauchy region is taken to be in the standard 3+1 form

$$ds^2 = -\alpha^2 dt^2 + h_{\alpha\beta}(dx^\alpha - N^\alpha dt)(dx^\beta - N^\beta dt). \tag{46}$$

where α is the lapse, N^α is the shift and $h_{\alpha\beta}$ is the spatial 3-metric. Coordinate conditions are used to simplify the form of the metric tensor and Einstein equations. In particular, θ and ϕ are chosen to represent spherical polar coordinates so that the off-diagonal components $h_{r\theta}$ and $h_{r\phi}$ vanish, and a radial gauge is employed in which

$$\det h_{AB} = r^4 \sin^2\theta, \tag{47}$$

where $A, B, \ldots = 2, 3$. The spatial metric can then be written in the form

$$h_{\alpha\beta}dx^{\alpha}dx^{\beta} = A^2dr^2 + r^2(B^{-2}d\theta^2 + B^2\sin^2\theta(d\phi + \xi\sin\theta)^2). \tag{48}$$

The quantity B is related to an auxiliary variable η via the definition

$$B^2 = 1 + \eta\sin^2\theta, \tag{49}$$

where η and ξ are the two independent polarisation amplitudes, h_+ and $h_\times$ respectively, of gravitational waves in the transverse traceless gauge,

$$h_+ := \eta\sin^2\theta, \qquad h_\times := -\sin^2\theta\int_0^t \alpha A^{-1}\xi, \tag{50}$$

for large values of the radial coordinate.

With these coordinate choices in place, the metric data which are evolved are the following:

$$\begin{array}{lll} \alpha, & & \text{(lapse)} \\ \beta^r = N^r/r, \quad G = N^\theta/\sin\theta, & N^\phi, & \text{(shift)} \\ A & & \text{(the radial metric component} \sqrt{h_{rr}}) \\ \eta, \quad \xi, & & \text{(wave-modes).} \end{array}$$

Extrinsic curvature components are projected onto a basis of orthonormal vectors,

$$e_{\mathbf{1}}^{\alpha} = [A^{-1}, 0, 0], \qquad e_{\mathbf{2}}^{\alpha} = [0, B/r, -\xi B\sin\theta/r], \qquad e_{\mathbf{3}}^{\alpha} = [0, 0, 1/(Br\sin\theta)], \tag{51}$$

so that the independent components of the extrinsic curvature in axially symmetry can be represented by the set

$$\begin{aligned} K_1 = K_{\mathbf{11}}, \qquad K_2 = K_{\mathbf{12}}, \qquad K_3 = K_{\mathbf{13}}, \\ K_+ = \frac{1}{2}(K_{\mathbf{33}} - K_{\mathbf{22}})/\sin^2\theta, \qquad K_\times = K_{\mathbf{23}}/\sin^2\theta, \end{aligned} \tag{52}$$

where the form of K_+ and $K_\times$ are chosen so that they represent the even and odd parity modes (in the linearised case) and are conjugate to η and ξ respectively.

The polar slicing condition

$$K = K^r{}_r, \tag{53}$$

is used in order to improve the behaviour of the metric variables at the interior ($r = 0$) and exterior boundaries, as well as simplify the integration of the field equations. It has a number of advantages over maximal slicing

$$K = 0, \tag{54}$$

since polar slicing involves a parabolic equation for the lapse which is much less expensive to solve numerically than the corresponding elliptical equation in maximal

slicing. Polar slicing also exhibits strong singularity avoiding properties, and when used in combination with the radial gauge results in a simple outer boundary condition on the lapse. However, at the origin (where maximal slicing has a perfectly well-defined lapse) the lapse is irregular for polar slicing. In order to take advantage of the benefits of both types of slicing, the trace of the extrinsic curvature is set as follows:

$$K = (1 - C(r))K_r{}^r, \tag{55}$$

where $C(r) = 1$ at the origin and decreases to zero before reaching the outer boundary. Significantly, the equation for the lapse is inward parabolic in the outer region where the spacetime is polar sliced, and switches to an elliptic equation as $C(r)$ becomes non-zero [35]. The lapse is thus solved inwards from the outer boundary, and its value at the edge of the elliptic region is used as a boundary condition for an elliptic solver acting over the inner maximally sliced region around the origin.

In the characteristic region we adopt a 2+2 null-timelike foliation and employ the parametrisation for the line element due to Bondi-Sachs [36], [37]

$$ds^2 = -(Ve^{2\beta}/r)du^2 - 2e^{2\beta}dudr + r^2h_{AB}(dx^A - U^Adu)(dx^B - U^Bdu), \tag{56}$$

where

$$h_{AB} = \begin{pmatrix} e^{2\gamma}\cosh 2\delta & \sinh 2\delta \\ \sinh 2\delta & e^{-2\gamma}\cosh 2\delta \end{pmatrix}. \tag{57}$$

The six metric functions $\{\gamma, \delta, \beta, U^2, U^3, V\}$ correspond to the six degrees of freedom remaining in the metric once four coordinate conditions have been applied, and have been chosen in such a way as to provide ready geometric and physical interpretations. Specifically, the variables δ and γ define the conformal geometry of the spacelike surfaces of constant radius and encode the two radiative degrees of freedom [1], $Ve^{2\beta}/r$ acts as a lapse function and $-U^A$ as a shift (see Fig. 12). The two line elements are specialised to axisymmetry by simply restricting all the metric variables to be independent of the azimuthal coordinate ϕ.

The form of the Bondi-Sachs metric has been derived by employing four algebraic coordinate conditions (namely $g^{00} = g^{02} = g^{03} = \det g_{AB} - r^4\sin^2\theta = 0$), whereas the axial form of the 3+1 metric has only involved three coordinate conditions (namely $h_{r\theta} = h_{r\phi} = \det h_{AB} - r^4\sin^2\theta = 0$). However, in this gauge, polar slicing can be thought of as a condition on one of the components of the shift (specifically N^2) [17]. With this insight, it proves possible to write down explicit formulae connecting the metric and its first derivatives at the interface [14]. It is then necessary to look in detail at the asymptotic character of the field equations [16]. We omit the details but give below an outline of the main algorithm for the CCM timestep on which the master axial code is built [38]. The code is currently being tested and evaluated.

1. Evolve η and ξ
2. Evolve the extrinsic curvature $K_1, K_2, K_3, K_+, K_\times$
3. Determine A via the Hamiltonian constraint
4. Evolve A independently as a check
5. Extract η, ξ, A and determine $\partial_u \delta, \partial_u \gamma$ on the interface I
6. Evolve δ, γ
7. Determine the asymptotic form of β on future null infinity $\mathcal{J}$
8. Determine β by inward integration
9. Inject β
10. Determine G, β^r, α
11. Extract $U, W, V, \partial_y U, \partial_y W$
12. Determine U, W, V by outward integration
13. Inject data to determine $\eta, \xi, K_1, K_2, K_3, K_+, K_\times, A, G$ on I
14. Repeat from Step 1 for the next time slice

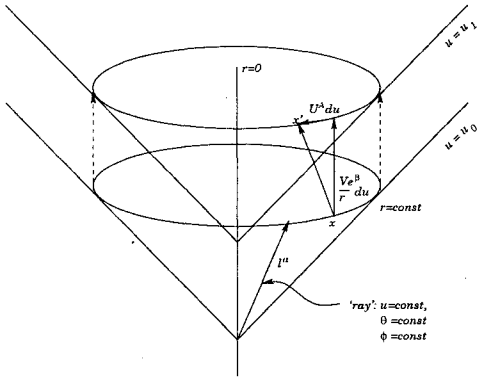

Figure 12: The Bondi-Sachs coordinate system fixes the coordinates to null rays of the spacetime, parametrised by the luminosity parameter r. The metric functions V and U^A act analogously to the lapse and shift in transporting coordinates from one r = constant slice to another.

References

[1] d'Inverno, R.A. and Stachel, J. *J. Math. Phys.*, 19, 1978, 2447.

[2] d'Inverno, R. A. and Smallwood, J. *Phys. Rev. D*, 22, 1980, 1233.

[3] Bishop, N.T., Gomez, R., Lehner, L. and Winicour, J. *Phys. Rev. D*, 54, 1986, 6153.

[4] Winicour, J. *Living Reviews*, (`http://www.livingreviews.org`), 1998.

[5] Friedrich, H. *Comm. Math. Phys.*, 91, 1983, 701.

[6] Clarke, C.J.S. and d'Inverno, R.A. *Class. Quantum. Grav.*, 11, 1994, 1463.

[7] Clarke, C.J.S., d'Inverno, R.A. and Vickers, J.A. *Phys Rev D*, 52, 1995, 6863.

[8] Dubal, M.R., d'Inverno, R.A. and Clarke, C.J.S. *Phys Rev D*, 52, 1995, 6868.

[9] Sjödin, K.R.P., Sperhake, U. and Vickers, J.A. Dynamic Cosmic Strings I, preprint gr-qc 0002096, 2000.

[10] Sperhake, U., Sjödin, K.R.P. and Vickers, J.A. Dynamic Cosmic Strings II, preprint gr-qc 0003114, 2000.

[11] Piran, T., Safier, P.N. and Katz. J. *Phys. Rev. D*, 34, 1986, 4919.

[12] Xanthopoulos, B.C. *Phys. Rev. D*, 34, 1986, 3608.

[13] Stark, R.F. and Piran, T. *Comput. Phys. Rep.*, 5, 1987, 221.

[14] d'Inverno, R.A. and Vickers, J.A. *Phys. Rev. D*, **54**, 1996, 4919.

[15] d'Inverno, R.A. *Class. Quantum Grav.*, 12, 1994, L75.

[16] d'Inverno, R.A. and Vickers, J.A. *Phys. Rev. D*, **56**, 1997, 772.

[17] d'Inverno, R.A. *Computer Phys. Comm.*, 115, 1998, 330.

[18] Jordan, P., Ehlers, J. and Kundt, W. *Abh. Wiss. Mainz. Math. Naturwiss.*, K1, 1960, 2.

[19] Kompaneets, A.S. *Sov.Phys. JETP*, 7, 1958, 659.

[20] Weber, J. and Wheeler, J.A. *Rev. Mod. Phys.*, 29, 1957, 509.

[21] Piran T., Safier, P.N. and Stark, R.F. *Phys. Rev. D*, 32, 1985, 3101.

[22] Zel'dovich, Y.B. *Mon. Not. R. astr. Soc.*, 192, 1980, 663.

[23] Vilenkin, A. and Everett, A E. *Phys. Rev. Lett.*, 48, 1982, 1867.

[24] Got, T. *Prog. Theor. Phys.*, 46, 1971, 1560.

[25] Garfinkle D. *Phys. Rev. D*, 32, 1985, 1323.

[26] d'Inverno, R.A., Dubal, M.R. and Sarkies, E.A. *Class. Quantum Grav.*, 17, 2000, 1.

[27] Dubal, M.R., d'Inverno, R.A. and Vickers, J.A. *Phys Rev D*, 58, 1998, 044019.

[28] Buchdahl, H.A. *Astrophys. J*, 140, 1964, 1512.

[29] Fletcher, C.A.J. *Computational Techniques for Fluid Dynamics Vol. II*, 1991, Springer-Verlag.

[30] Oohara, K. and Nakamura, T. *Prog. Theor. Phys.*, 88, 1992, 1079.

[31] Shibata, N., Nakamura, T. and Oohara, K. *Prog. Theor. Phys.*, 89, 1993, 809.

[32] Gunnarsen, L., Shinkai H-A. and Maeda, K-I. *Class. Quantum Grav.*, 12, 1995, 133.

[33] d'Inverno, R.A. and Russell-Clark, R.A. *J. Math. Phys.*, 12, 1971, 1258.

[34] d'Inverno, R.A. and Vickers, J.A. Combining Cauchy and characteristic codes. Using principal null directions as a visualisation tool in Numerical Relativity, (in preparation).

[35] Bardeen J.M. and Piran, T. *Phys. Rep.*, 96, 1983, 205.

[36] Bondi, H., van der Burg M.G.J. and Metzner, A.W.K. *Proc. Roy. Soc.*, A269, 1962, 21.

[37] Sachs, R.K. *Proc. Roy. Soc.*, A270, 1962, 103.

[38] Pollney, D. PhD Thesis, University of Southampton, 2000.